

Clemson University

**TigerPrints**

---

Open Access Publishing Fund

---

6-1-2022

## Global Flash Drought Analysis: Uncertainties From Indicators and Datasets

Sourav Makherjee  
*Clemson University*

Ashok Kumar Mishra  
*Clemson University*

Follow this and additional works at: [https://tigerprints.clemson.edu/oa\\_fund](https://tigerprints.clemson.edu/oa_fund)

---

### Recommended Citation

Mukherjee, S., & Mishra, A. K. (2022). Global flash drought analysis: Uncertainties from indicators and datasets. *Earth's Future*, 10, e2022EF002660. <https://doi.org/10.1029/2022EF002660>


This Article is brought to you for free and open access by TigerPrints. It has been accepted for inclusion in Open Access Publishing Fund by an authorized administrator of TigerPrints. For more information, please contact [kokeefe@clemson.edu](mailto:kokeefe@clemson.edu).

# Earth's Future

## RESEARCH ARTICLE

10.1029/2022EF002660

# Global Flash Drought Analysis: Uncertainties From Indicators and Datasets

Sourav Mukherjee<sup>1</sup>  and Ashok Kumar Mishra<sup>1</sup> 

<sup>1</sup>Glenn Department of Civil Engineering, Clemson University, Clemson, SA, USA

### Key Points:

- Two unique Flash Drought (FD) indicators reveal disparate FD characteristics and climate controls of FDs
- Meteorological forcings and soil-temperature coupling show a varied impact on FD evolution depending on the datasets used
- Robust methodologies should simultaneously capture the rapid increase in evaporative stress and soil moisture depletion rates

### Supporting Information:

Supporting Information may be found in the online version of this article.

### Correspondence to:

A. K. Mishra,  
ashokm@g.clemson.edu

### Citation:

Mukherjee, S., & Mishra, A. K. (2022). Global flash drought analysis: Uncertainties from indicators and datasets. *Earth's Future*, 10, e2022EF002660. <https://doi.org/10.1029/2022EF002660>

Received 11 JAN 2022

Accepted 27 MAY 2022

### Author Contributions:

**Conceptualization:** Sourav Mukherjee, Ashok Kumar Mishra  
**Formal analysis:** Sourav Mukherjee  
**Funding acquisition:** Ashok Kumar Mishra  
**Investigation:** Sourav Mukherjee  
**Methodology:** Sourav Mukherjee, Ashok Kumar Mishra  
**Supervision:** Ashok Kumar Mishra  
**Validation:** Sourav Mukherjee  
**Writing – original draft:** Sourav Mukherjee

© 2022 The Authors. Earth's Future published by Wiley Periodicals LLC on behalf of American Geophysical Union. This is an open access article under the terms of the [Creative Commons Attribution-NonCommercial-NoDerivs License](https://creativecommons.org/licenses/by/4.0/), which permits use and distribution in any medium, provided the original work is properly cited, the use is non-commercial and no modifications or adaptations are made.

**Abstract** Flash Drought (FD) has garnered much attention in recent years, with significant advancements in the indicators applied for identifying these rapidly intensifying events. However, the difference in existing FD definitions and methodologies among research communities and the choice of different data sources underscores the importance of addressing the uncertainties associated with the global FD characteristics and their drivers. This study compares two key FD indicators derived based on evaporative stress ratio (ESR) and root-zone soil-moisture (RZSM) using three different data sources to investigate the uncertainties in global FD frequency and intensity (speed), and the influencing drivers. The results suggest that such disparities are significant in the two FD indicators across different climate regions of the globe. The results highlight varying spatial drivers of FD frequency, intensity, and their evolution, potentially linked to background aridity. Changes in precipitation, temperature, vapor pressure deficit, and soil-temperature coupling play an important role with a cascading (concurrent) impact on the evolution of FD based on RZSM (ESR). The relationship between ESR and RZSM fails to explain most of the variance in each of these indicators specific to the FD episodes, especially in the transitional and humid climate regimes. Overall, the results highlight the necessity of more nuanced methodologies for deriving FD indicators that can efficiently couple the rapid soil-moisture depletion rates in deeper layers with changes in atmospheric evaporative demand which has direct implications on vegetation health.

## 1. Introduction

Drought is a complex and extreme climatic condition leading to significant impact on water availability, socio-economic systems, and environmental sustainability (A. K. Mishra & Singh, 2010; Mukherjee et al., 2018). Flash droughts (FDs), unlike slow evolving drought events, are characterized by sudden and rapid intensification within a few pentads or weeks. The FD events are generally unforeseen and can cause devastating socio-economic impacts quickly (Ford & Labosier, 2017; Jin et al., 2019; Lisonbee et al., 2021; Mallya et al., 2013; Otkin et al., 2016). For instance, the inflation-adjusted cost of the 2012 summer flash drought in the US is estimated to exceed \$30 billion across the nation (<https://www.ncdc.noaa.gov/billions/>; Chen et al., 2019). The US Drought Monitor reported that between April and September 2017, severe flash droughts in North America resulted in 25% reduction in cropland evapotranspiration, 6% decrease in crop production, and 11% reduction in solar-induced chlorophyll fluorescence productivity over the region relative to the longer (2008–2017) satellite record causing massive losses to the agricultural industry (He et al., 2019).

FDs are mainly driven by the co-evolution of low precipitation and high temperature conditions that favors the rapid intensification of atmospheric evaporative demand, and soil moisture depletion rates (Apurv & Cai, 2020; Mo & Lettenmaier, 2015; Otkin et al., 2018; Pendergrass et al., 2020; Wang et al., 2016). Although a handful of scientific literature investigated the occurrence and underlying causes of FDs across various parts of the globe, there is limited consensus among them in the way the FD events are defined (Christian et al., 2020; Lisonbee et al., 2021; Mahto & Mishra, 2020; Mo & Lettenmaier, 2016; Otkin et al., 2018; Svoboda et al., 2002; L. Wang et al., 2016; Yuan et al., 2019). More precisely, the major disparity among these literature is their reliance on distinct indicators that define FDs.

So far, FDs have been defined based on several indicators, such as evaporative stress ratio (ESR) (Christian, Basara, Otkin, & Hunt, 2019; Christian, Basara, Otkin, Hunt, et al., 2019; Otkin et al., 2018), soil moisture estimates (Mahto & Mishra, 2020; Mukherjee & Mishra, 2022; V. Mishra et al., 2021; Yuan, Zheng, et al., 2019), the U.S. Drought Monitor (Chen et al., 2019; Svoboda et al., 2002), Evaporative Demand Drought Index (Parker et al., 2021), and Standardized Precipitation Index (Lisonbee et al., 2021; Noguera et al., 2021). In this study,

Writing – review & editing: Ashok Kumar Mishra

we selected standardized ESR (SESR) and root-zone-soil-moisture (RZSM) to define FDs due to their overwhelming use in recent years (Lisonbee et al., 2021; Pendergrass et al., 2020). Both SESR and soil-moisture have been applied globally for defining FDs (Christian et al., 2021; Koster et al., 2019). ESR directly incorporates the near-surface state variables and is relevant for monitoring the direct impact of FD on vegetation (Anderson et al., 2016; Otkin et al., 2018; Pendergrass et al., 2020), while soil moisture is a useful indicator for FD forecasting (Ford et al., 2015; McColl et al., 2017; Otkin et al., 2016).

Some of the canonical flash drought definitions, applied for specific regions, are found to have some resemblance in the spatial coverages, however, these definitions yield substantially disparate results in the assessment of the occurrences, duration and timing of notable flash droughts (Osman et al., 2020; Yuan, Zheng, et al., 2019). Furthermore, differences in adopted definition, input variables, and methodologies of flash drought may impact the assessment of the effect of climate anomalies and surface energy fluxes that significantly control the hydrological cycle (Beltrami & Kellman, 2003; Entekhabi et al., 1996; Forzieri et al., 2020; Hao et al., 2018; Ionita et al., 2017; Konapala et al., 2020). Additionally, the use of different data sets (sources) for deriving ESR and soil moisture estimates can lead to significant uncertainties in determining FD characteristics and their potential drivers over a given region. Although, ensemble approach using multiple datasets have been implemented for assessing global distribution, trends and drivers of FDs (Christian et al., 2021), data related uncertainties remain underexplored. In the light of such limitations, it is essential to address such uncertainties arising from both methodological and data-related disparities (Hoffmann et al., 2020).

This study aims to address the uncertainties associated with FD frequency, rate of intensification, and the influence of climate anomalies and background aridity on FD evolution across the globe using two distinct FD indicators, SESR and root-zone-soil moisture (RZSM). We compared three different reanalysis and model-derived datasets for FD characterization. Overall, we aim to answer the following questions.

1. Which regions show higher FD frequency and intensity uncertainties based on two FD indicators (SESR and RZSM) derived using the three different data sources, GLEAM, ERA5, and MERRA2?
2. How do the climate control global FD evolution based on two distinct FD indicators and different datasets?
3. What is the effect of background aridity on the relationship between SESR and RZSM specific to the FD episodes based on the two different FD indicators.
4. What are the uncertainties associated with the most dominant climate precursors of FD intensity in different evaporation regimes of the globe?

This paper is structured as follows. Section 2 describes the datasets used in the study, followed by methodology in Section 3. The results are provided in Section 4, and the discussion and conclusion in Section 5.

## 2. Data

SESR is derived at pentad scale for the period 1980 to 2018 using daily ESR. The daily values of ESR are calculated using global gridded daily actual evapotranspiration (AET) and potential evapotranspiration (PET) dataset obtained from the three different data sources, third version of the Global Land and Evaporation Amsterdam Model (GLEAM v3.3a; Miralles et al. (2011)) available at <https://www.gleam.eu/>, European Centre for Medium-Range Weather Forecasts Reanalysis 5 (ERA5), and Modern-Era Retrospective Analysis for Research and Applications, Version 2 (MERRA2). Daily RZSM is obtained directly from the three data sources (GLEAM v3.3a, ERA5, and MERRA2). The GLEAM v3.3a dataset spans between 1980 and 2018 and is available daily for every  $0.25^\circ \times 0.25^\circ$  pixels globally. The ERA5 (MERRA2) datasets are available at  $0.25^\circ \times 0.25^\circ$  ( $0.5^\circ \times 0.625^\circ$ ) pixels. The daily PET dataset, provided by GLEAM, is generated based on the Priestley and Taylor (PT) evaporation model. Unlike GLEAM, daily PET data is not available directly from ERA5, and MERRA2. Therefore, PET based on ERA5, and MERRA2 data was calculated separately using the Priestley and Taylor (PT) evaporation model (see Text S1 in Supporting Information S1) to maintain consistency with the PET data provided by GLEAM.

Global evaporation regimes are identified based on Aridity index (AI) calculated using mean annual precipitation and PET datasets obtained from the ERA5 (see Text S2 in Supporting Information S1). To investigate the climate controls of FD frequency, evolution, and intensity, we selected four different climate and hydrological variables, such as precipitation (Pr), daily maximum 2-m temperature (tmax), vapor pressure deficit (VPD), and

soil-moisture temperature coupling (denoted as  $\pi$ ). The association of FD with these variables were evaluated separately using data from two different reanalysis datasets, ERA5, and MERRA2. In addition to exploring data related uncertainties, the use of these two reanalysis datasets also meets the need for atmospheric reanalysis, which are not available in the dataset provided by GLEAM. A brief discussion on the calculation of VPD, and  $\pi$  is provided in Text S3 and S4 in Supporting Information S1. To maintain consistency, all datasets were regridded to a common  $0.5^\circ \times 0.5^\circ$  grid resolution using a bilinear interpolation scheme.

### 3. Methodology

#### 3.1. Flash Drought Identification

Flash droughts are characterized by the rapid intensification of drought conditions over a short period. In this study, flash drought events are identified based on two different methodologies, (a) based on SESR ( $FD_{SESR}$ ) proposed by Christian, Basara, Otkin, Hunt, et al. (2019) and (b) based on RZSM ( $FD_{RZSM}$ ) proposed by Yuan, Zheng, et al. (2019), as discussed below.

##### 3.1.1. $FD_{SESR}$ Detection Methodology

This methodology relies upon the concept of evaporative stress ratio (ESR (Anderson et al., 2007a, 2007b; Christian, Basara, Otkin, & Hunt, 2019; Christian, Basara, Otkin, Hunt, et al., 2019; Christian et al., 2021), which is calculated based on the ratio between AET and PET as,

$$ESR = \frac{AET}{PET} \quad (1)$$

where  $ESR$  ranges from zero to approximately one, such that  $ESR$  approaching zero generally indicates a very high atmospheric demand for evaporation that is hardly met by the available soil moisture, thus, implying the presence of very high evaporative stress on the environment and vice versa.

The standardized  $ESR$  ( $SESR$ ) values are used to identify flash droughts at the pentad (5-day) scale. Mean pentad (or 5-day average) values of  $ESR$  were calculated and then standardized for each grid point as (Christian, Basara, Otkin, & Hunt, 2019; Christian, Basara, Otkin, Hunt, et al., 2019),

$$SESR_{ijp} = \frac{ESR_{ijp} - \overline{ESR}_{ijp}}{\sigma_{ESR_{ijp}}} \quad (2)$$

where  $SESR_{ijp}$  (hereafter referred to as SESR) is the z score of the ESR at a specific grid point (i, j) for a specific pentad p,  $\overline{ESR}_{ijp}$  is the mean ESR at a particular grid point (i, j) for a specific pentad p for all years available in the gridded dataset (here, from 1980 to 2018), and  $\sigma_{ESR_{ijp}}$  is the standard deviation. Subsequently, the temporal change in SESR was calculated and standardized as,

$$(\Delta SESR_{ijp}) = \frac{\Delta SESR_{ijp} - \overline{\Delta SESR}_{ijp}}{\sigma_{\Delta SESR_{ijp}}} \quad (3)$$

where  $(\Delta SESR_{ijp})_z$  (hereafter referred to as  $\Delta SESR$ ) is the z score of the change in SESR at a specific grid point (i, j) for a particular pentad p for all years available in the gridded dataset and  $\sigma_{\Delta SESR_{ijp}}$  is the standard deviation. The SESR and  $\Delta SESR$  magnitudes are finally applied to identify the flash drought events following a set of criteria and estimate the intensity of those events worldwide. The criteria are summarized as.

1. Flash drought events are required to have a minimum length of five SESR changes  $\Delta SESR$ , which is equivalent to a duration of six pentads (30 days).
2. A final SESR value below the twentieth percentile of SESR values.
3. The  $\Delta SESR$  value must be at or below the 40th percentile between individual pentads, and no more than one  $\Delta SESR$  above the 40th percentile following a  $\Delta SESR$  that meets the former criterion.

4. The mean change in SESR ( $\Delta SESR$ ) during the entire duration of the flash drought must be less than the 25th percentile of the climatological changes in SESR for that grid point and time of year.

A detailed explanation of the methodology adopted for calculating the  $FD_{SESR}$  intensity is provided in Text S5 in Supporting Information S1. The standardized values, SESR can easily compare the evaporative stress between regions as well as evaporation regimes. Besides, SESR can be useful for robust comparison over multiple years and during the growing season for agricultural applications. It is further necessary to note that flash droughts can be identified in different ways (Otkin et al., 2018; Yuan, Zheng, et al., 2019). The SESR based analysis has a key advantage as it directly incorporates the near-surface state variables (e.g., air temperature, wind speed, vapor pressure deficit, latent and sensible heat fluxes, soil moisture, precipitation, and shortwave radiation), which are crucial for capturing the onset, intensification, and end of flash drought (Christian, Basara, Otkin, & Hunt, 2019; Christian, Basara, Otkin, Hunt, et al., 2019; Otkin et al., 2018).

### 3.1.2. $FD_{RZSM}$ Detection Methodology

The  $FD_{RZSM}$  events are derived based on existing methodology (Yuan, Zheng, et al., 2019) that combines the criteria of rapid decline in RZSM and dry persistency. In this methodology, the detection of  $FD_{RZSM}$  is employed based on the following three criteria (Yuan, Zheng, et al., 2019):

1. The pentad mean RZSM decreases from above 40th percentile to twentieth percentile, with an average decline rate of not less than 5% in RZSM percentiles for each pentad.
2. The FD is considered to have terminated if the declined RZSM rises up to twentieth percentile again. These two criteria determine a FD onset and termination stages.
3. The drought should last for at least 3 pentads (15 days).

The key advantage of this methodology lies in its ability to capture rapid changes in drying and high sensitivity toward the termination of drought events from rain. However, the existing methodology does not provide a metric for calculating the FD intensity. The methodology applied to calculate the  $FD_{RZSM}$  intensity is discussed in Text S5, and Table S1 in Supporting Information S1.

## 3.2. Random Forest Algorithm

Random Forest (RF) is a robust Machine Learning algorithm that works on ensemble learning method for classification and regression trees (Breiman, 2001) and have been extensively used for drought monitoring and forecasting studies (Deo et al., 2017; Konapala & Mishra, 2020; Park et al., 2016; Rhee & Im, 2017; Sutanto et al., 2019). We used the RF model to evaluate the order of variable importance due to the high accuracy of the algorithm and it avoids overfitting and efficiently deals with multicollinearity.

The order of variable importance in a RF model is determined based on the percentage increase in mean squared error (%IncMSE) of prediction corresponding to each predictor variable. The %IncMSE is considered as the most robust and informative measure for feature selection in a RF model. The number of independent trees (in our Case 500) are selected based on trace plots (not shown) of the %MSE. In our analysis, the RF model is employed for each evaporation regime, separately, with the yearly mean FD intensity (excluding those with zero events) as the decision variable and corresponding lagged (0, 1, 2 pentads) yearly mean of standardized anomalies of Pr, Tmax, VPD, and pi as the predictors for individual grids. The RF model is fitted on yearly values of mean FD intensity and the predictor variables pooled together from all grid locations within a regime. This method of pooling data together produces enough sample size that facilitates robust predictions and help to represent wholistic dynamics of the FD system within the evaporation regimes. Additionally, it is important to note that in the analysis, the selection of FD years for a given FD definition and regime is same across all predictor variables among whom the prediction efficacies are compared.

## 4. Results

### 4.1. Uncertainties in Global $FD_{SESR}$ and $FD_{RZSM}$ Characteristics

We investigated the disparities and data-related uncertainties associated with  $FD_{SESR}$  and  $FD_{RZSM}$  frequency and mean intensity across the globe at  $0.5^\circ \times 0.5^\circ$  grid resolution. To explore methodological and data-related



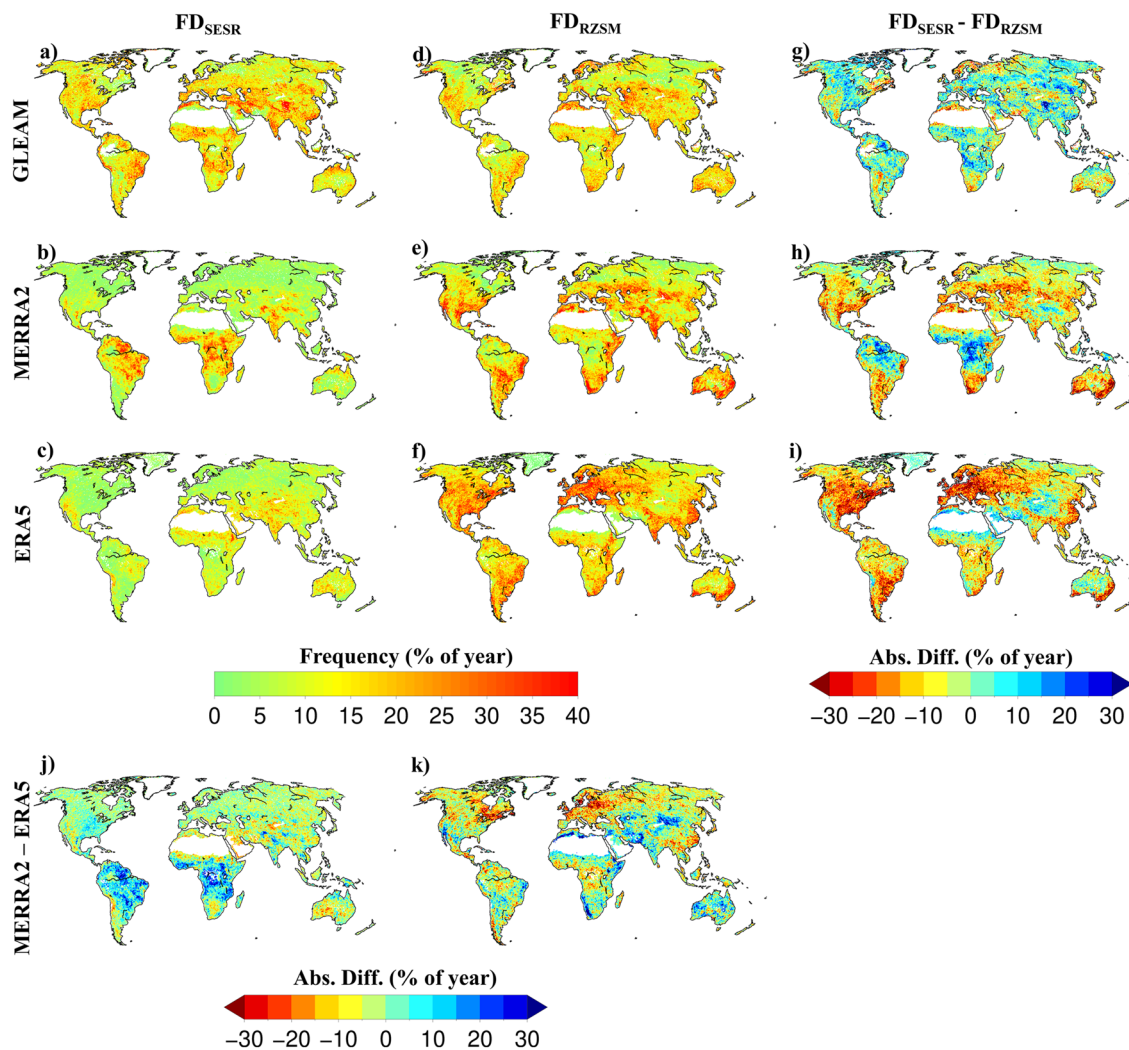


**Figure 1.** (a–k) Spatial maps (a–c) showing the frequency of occurrence of Flash Drought ( $FD_{SESR}$ ), as percent of years for 1980–2018 period based on (a) Global Land and Evaporation Amsterdam Model (GLEAM), (b) Modern-Era Retrospective Analysis for Research and Applications, Version 2, and (c) European Centre for Medium-Range Weather Forecasts Reanalysis 5 (ERA5) data set, (d–f) same as in (a–c) but for  $FD_{RZSM}$ . (g–i) absolute differences (%) in the frequency of  $FD_{SESR}$  and  $FD_{RZSM}$  occurrences, (j) absolute differences between  $FD_{SESR}$  frequency as in MERRA and ERA5 data set, and (k) same as in (j) but for  $FD_{RZSM}$ .

uncertainties, the  $FD_{SESR}$  and  $FD_{RZSM}$  frequency and intensity are derived separately for 1980–2018 and compared using three different datasets, GLEAM, ERA5, and MERRA2 datasets. A detailed explanation for the procedures applied for both  $FD_{SESR}$  and  $FD_{RZSM}$  event detection, and calculation of event intensity are provided in the Methods section. Figures 1a–1f illustrates the global distribution of  $FD_{SESR}$  and  $FD_{RZSM}$  frequency calculated as the percentage of years between 1980 and 2018 that witnessed at least one FD event. The disparities associated with the frequency exhibited by these two FD indicators are shown in Figures 1g–1i, which is calculated as the absolute difference between the  $FD_{RZSM}$  and  $FD_{SESR}$  frequency based on each of the datasets. The data related uncertainties between the MERRA2 and ERA5 are illustrated in Figures 1j and 1k. Similarly, the global distribution of the  $FD_{RZSM}$  and  $FD_{SESR}$  mean intensity and related uncertainties is depicted in Figure S1 in Supporting Information S1.

Substantial disparities can be noted due to methodological differences stemming from two distinct indicators (SESR, and RZSM) over the global land areas for any given datasets. For instance, in the GLEAM dataset, significant differences can be noted over the US between the  $FD_{SESR}$  and  $FD_{RZSM}$  occurrences, where  $FD_{SESR}$  occurrences are found to be 15%–20% higher in the humid southeastern parts of the US (Figure 1g). On the other hand,  $FD_{RZSM}$  occurrences are found to be 10%–15% higher in the northern parts of Europe, and Asia, some parts

of central Asia, southernmost Africa, and Australia. Similarly, in the MERRA2 data set, while regions like central Africa and the northern half of South America exhibit more than 20% higher occurrences of  $FD_{SESR}$  events, the occurrences of  $FD_{RZSM}$  events are found to be more than 20% higher in majority of the global land area, such as in the US, central and southern parts of Europe, central Asia, southern parts of South America, Africa, and Australia. Even higher disparities between the  $FD_{RZSM}$  and  $FD_{SESR}$  occurrences are exhibited in the ERA5 datasets.  $FD_{RZSM}$  event occurrences are found to be more than 25% higher in the majority of the globe, including entire US, Europe, humid regimes of eastern China, Western Asia, and Southern parts of South America, Africa, and Australia. In addition to that, striking disparities can be noted between the mean intensity of  $FD_{SESR}$  and  $FD_{RZSM}$  events across the whole globe (Figure S1 in Supporting Information S1).

Although flash drought frequency, particularly in the Great Lakes Region, western North America, and South-eastern China, matches well with respect to the indicators, such as, ESR, and different soil moisture indices, used to capture the regional patterns reported in previous studies (Christian, Basara, Otkin, & Hunt, 2019; Christian, Basara, Otkin, Hunt, et al., 2019; Christian et al., 2021; Osman et al., 2020; L. Wang et al., 2016), there are substantial data related inconsistencies for a given indicator. Data-related uncertainties can be noted across several parts of the globe, mainly corresponding to the  $FD_{SESR}$  methodology. The GLEAM data set exhibits substantially higher occurrences and mean intensity of FD events than both ERA5 and MERRA2. On the other hand, such uncertainties are relatively lower in the case of  $FD_{RZSM}$ , with relatively higher agreement in both FD frequency and intensity across the MERRA2 and ERA5 data sets (Figure 1 and S1 in Supporting Information S1). Such uncertainties can result from disparities in land-surface models and data assimilation techniques applied in the MERRA2 and ERA5 datasets (Hersbach et al., 2020; Martens et al., 2020; Reichle et al., 2017).

Besides,  $FD_{SESR}$  and  $FD_{RZSM}$  frequencies show a relatively higher agreement in the GLEAM datasets (Figures 1a–1c). Such agreements can be noted for regions located over the west, east, and southern Asia, northern and southern parts of North America, southeastern parts of South America, and majority of the African continent. These results also align with the goal of GLEAM project in representing land surface processes more accurately as compared to the MERRA2 and ERA5 reanalysis whose primary goal is to represent the atmospheric processes more accurately. Therefore, to further investigate the methodological uncertainties associated with the climate controls and key drivers of  $FD_{SESR}$  and  $FD_{RZSM}$  evolution, we use the GLEAM data set as a control experiment for deriving the  $FD_{SESR}$  and  $FD_{RZSM}$  characteristics and derive the climate anomalies from the ERA5 and MERRA2 datasets.

#### 4.2. Climate Controls of $FD_{SESR}$ and $FD_{RZSM}$ Evolution

Droughts are primarily triggered by climatic perturbations (Hanel et al., 2018; Ionita et al., 2017; Konapala et al., 2020) and atmospheric evaporative demand (Parker et al., 2021; Vicente-Serrano et al., 2020), causing rapid intensification of evaporative stress and soil moisture depletion leading to flash droughts. However, such effects can be complex, and their influence can differ, varying from cascading to compounding in nature (Christian et al., 2020; Raymond et al., 2020; Zscheischler et al., 2020). We investigate such differences in the influence of climate anomalies on SESR, and RZSM depletion rates associated with the evolution of FDs for global land areas during the 1980–2018 period.

We selected pentad mean of daily total precipitation ( $Pr$ ), maximum 2m air temperature ( $T_{max}$ ), vapor pressure deficit ( $VPD$ ), and soil-temperature coupling strength ( $\pi$ ) (Miralles et al., 2012; Seneviratne et al., 2010) up to four lagged pentads, and three pentads after the FD onset. All of these climate variables are available and obtained from two different reanalysis datasets, ERA5 and MERRA2, to explore the robustness of the results. The standardized anomalies of each of these variables are derived with respect to their climatological pentad mean (for the 1980–2018 period). The procedures followed for calculating  $VPD$  and  $\pi$  are discussed in the supplementary (Text S3, and S4 in Supporting Information S1). The FD onset timings are determined using the GLEAM datasets as the control experiment to explore the methodological disparities among the influence of these climate anomalies on the  $FD_{SESR}$  and  $FD_{RZSM}$  evolution. The total counts of  $FD_{SESR}$  and  $FD_{RZSM}$  events are calculated at each pixel ( $0.5^\circ \times 0.5^\circ$ ) and subsequently binned as a function of the standardized anomalies of each variable corresponding to the selected pentads as illustrated by 2D-contour plots in Figure 2 and Figure S2 in Supporting Information S1 based on ERA5 and MERRA2 datasets, respectively. Furthermore, weighted average of the standardized anomalies were calculated based on the event counts (shown by the shaded 2D-contours) for each

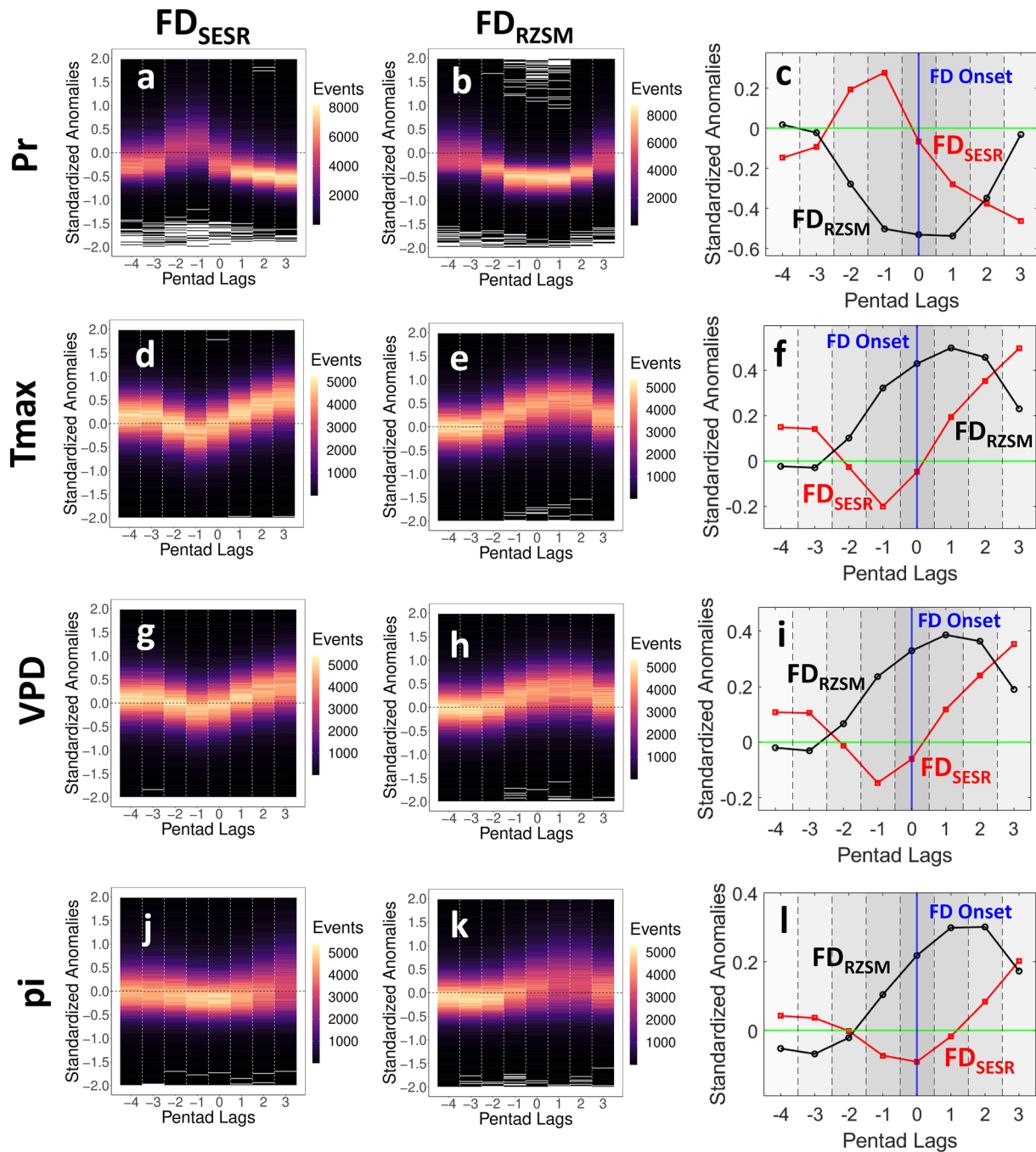


**Figure 2.** (a and b) Contour plots illustrating the total number of (a) Flash Drought (FD<sub>SES</sub>R) and (b) FD<sub>RZSM</sub> events binned as a function of standardized Pr anomalies (y-axis) in European Centre for Medium-Range Weather Forecasts Reanalysis 5 (ERA5) data set for first, second, third, and fourth pentad before (denoted by  $-4$  to  $-1$  in the x-axis) and first, second, and third pentad after (denoted by  $1-3$  in the x-axis) the onset of Flash Drought (FD) events (denoted by  $0$  in the x-axis), (c) temporal evolution of event-count weighted mean of standardized anomalies of Pr corresponding to FD<sub>SES</sub>R and FD<sub>RZSM</sub> episodes, (d-f) same as in (a-c) but for standardized anomalies of Tmax, (g-i) same as in (a-c) but for standardized anomalies of vapor pressure deficit (VPD), and (j-l) same as in (a-c) but for standardized anomalies of pi.

of the selected pentads to produce a time-series of the hydroclimatic anomalies, as shown in Figure 2 and S2 in Supporting Information S1.

The 2D-contour and time-series plots shown in Figure 2 (and Figure S2 in Supporting Information S1) suggest distinct types of association between the climate anomalies and FD onset and propagation in the two definitions.



While the onset and evolution of  $FD_{SES}$  show simultaneous development with changes in climate anomalies, a delayed or cascading effect of such climate anomalies is noted on the onset and evolution of  $FDR_{ZSM}$ . For example, for majority of  $FD_{SES}$  events, the climate anomalies and SESR anomalies intensify at the same time as the FD evolves. The magnitude of the anomalies corresponding to the maximum number of (about 5000)  $FD_{SES}$  events are observed to increase (or decrease in case of Pr) continuously from one pentad before the FD onset and reaches the peak (lowest) magnitude after three pentads from the FD onset. In contrast, the climate anomalies corresponding to the majority of the  $FD_{RZSM}$  events increase (or decrease in case of Pr) continuously two pentads before the FD onset, and reaches the peak (lowest) magnitude after one pentad of the FD onset, and thereafter decreases (increases for Pr) again. This behavior is even more prominent in the event weighted mean of the standardized anomalies for all the selected climate variables, Pr, Tmax, VPD, and pi, in both ERA5 and MERRA2 datasets. These results are consistent with the spatial maps shown in Figure S3–S4 and Figure S5–S6 in Supporting Information S1 for  $FD_{SES}$  and  $FD_{RZSM}$ , respectively.

Overall, our results are in close agreement with regional studies that suggest a similar spatio-temporal pattern of climatic forcings specific to FD onset and evolution corresponding to the indicators used (ESR or RZSM) (Christian et al., 2020; Ford & Labosier, 2017). This disparate behavior underscores the effect of soil-moisture memory, which is why climate anomalies have a delayed or cascading impact on  $FD_{RZSM}$  evolution (Hagemann & Stacke, 2015; Liang & Yuan, 2021; Seneviratne et al., 2006). On the other hand, the  $FD_{SES}$  events will be most likely to occur if there is a quick burst in precipitation that leads to enhanced ET but not enough to provide lasting improvement.

### 4.3. Effect of Background Aridity on $FD_{SES}$ and $FD_{RZSM}$ Intensification

The underlying mechanisms and drivers of drought can be complex and are potentially dependent on the background aridity that regulates the type of control (energy-limited or water-limited) on surface evaporation over a region (Forzieri et al., 2020; Mukherjee et al., 2018; Mukherjee & Mishra, 2021; Seneviratne et al., 2010; Su et al., 2021). As such, it is essential to understand the effect of background aridity on the (a) association between RZSM and ESR specific to all FD episodes and (b) uncertainties associated with the key drivers of FDs, represented by two distinct FD indicators (ESR and RZSM). In the following sections we explore these associations by dividing the global regions into four different evaporation regimes, arid, semi-arid, sub-humid, and humid regimes. The evaporation regimes were identified based on the aridity index (AI; see Text S4, Table S2 and Figure S7 in Supporting Information S1).

#### 4.3.1. Sensitivity of ESR and RZSM Relationship to Changes in Background Aridity

Investigating the association between the ESR and RZSM depletion for a given FD definition is necessary to understand how these variables interact over time as the FD evolves. More importantly, due to the considerable control of background aridity over drying rates, the association between ESR and RZSM, even for a given FD definition, may vary with changes in background aridity. We investigate sensitivity of these associations in response to changes in background aridity which is examined based on all FD episodes detected during the period 1980–2018 for a given FD definition. We select two distinct scenarios, scenario 1: Considering  $FD_{SES}$  episodes, and scenario 2: Considering  $FD_{RZSM}$  episodes, and explore these relationships independently. The choice of independent scenarios makes it possible to investigate the temporal association between ESR and RZSM within a given FD definition, even though the duration or pentads of FDs across different definitions may not exactly match or coincide at multiple locations (Figure S8 in Supporting Information S1). The FD episodes derived from the GLEAM data set are used in this analysis as a baseline for comparison, as they show relatively higher agreement in spatial patterns between  $FD_{SES}$  and  $FD_{RZSM}$  frequency as compared to that in the ERA5 and MERRA2 datasets (Figure 1).

The effect of background aridity on such associations is explored by evaluating the variance explained explicitly to the  $FD_{SES}$  and  $FD_{RZSM}$  episodes across the globe and over the different climate regimes, selected based on the aridity index. For instance, using scenario 1, we evaluate the proportion of variance in ESR explained by RZSM specific to the  $FD_{SES}$  episodes which is calculated based on the squared correlation coefficient ( $R^2$ ). Similarly, using scenario 2, we evaluate the proportion of variance in RZSM explained by ESR specific to the  $FD_{RZSM}$  episodes. By definition,  $R^2$  is the percentage of variance in a dependent variable explained by the linear regression equation (or relationship) between independent and dependent variables. A higher value of  $R^2$  indicates

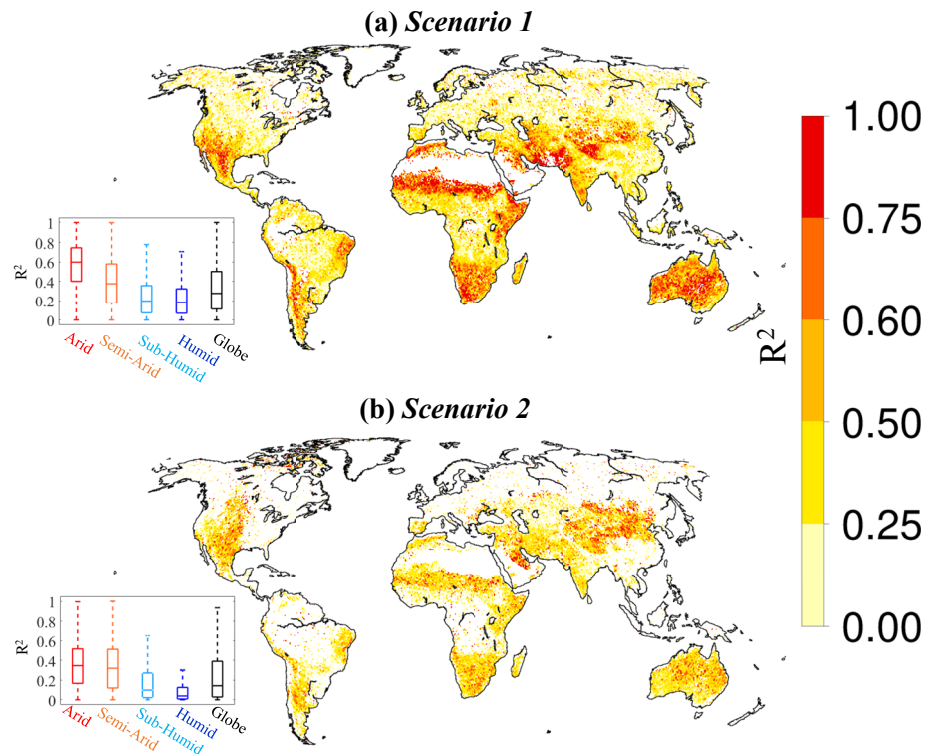


**Figure 3.** (a) Spatial map illustrating the global distribution of statistically significant (at 95% confidence level)  $R^2$  values corresponding to the relationship between evaporative stress ratio (ESR) and root-zone soil-moisture (RZSM) specific to the  $FD_{SESR}$  episodes with RZSM as the independent and ESR as the dependent variable in the linear regression (scenario 1), and boxplots showing the spatial distribution of these  $R^2$  values over the different climate regimes, (b) same as in (a) but specific to the  $FD_{RZSM}$  episodes with ESR as the independent and RZSM as the dependent variable in the linear regression (scenario 2).

a greater proportion of the variance explained. The  $R^2$  is estimated for every global grid location considering pentad-to-pentad values of ESR and RZSM during all FD episodes. For a given grid location, the  $R^2$  value is estimated using the individual pentads within all the flash drought events corresponding to a specific FD definition,  $FD_{SESR}$  and  $FD_{RZSM}$ , represented by two independent scenarios, scenario 1, and scenario 2, respectively. In the first scenario, both ESR values and RZSM percentiles were extracted for the  $FD_{SESR}$  pentads for the full period, 1980–2018. The  $R^2$  values were subsequently calculated using a linear regression approach using the extracted ESR time-series as the dependent variable and the extracted RZSM time-series as the independent variable. For the second scenario, both ESR values and RZSM percentiles were extracted similarly but for the  $FD_{RZSM}$  pentads. The  $R^2$  values were subsequently calculated based on a linear regression approach using the extracted time-series of RZSM as the dependent variable and the extracted time-series of ESR as the independent variable.

Figure 3 demonstrates the statistically significant (at 95% confidence level)  $R^2$  values evaluated based on the two scenarios for the whole globe and for the different climate regimes, selected based on the aridity index. The spatial map in Figures 3a and 3b suggest that the association between RZSM and ESR for both scenarios are sensitive to changes in background aridity. This is explained by the spatial distribution of  $R^2$  values shown by boxplots for the climate regimes. The proportions of explained variance are substantially greater in the arid regions and gradually decrease in the wetter regimes for both scenarios. For example, the median  $R^2$  value in the arid regimes for the scenario 1 (scenario 2) is about 0.6 (0.37), which suggests that the association between RZSM and ESR explains 60% (37%) of the variance in ESR (RZSM). On the other hand, the median  $R^2$  in the humid regions is less than 0.2. These results are in agreement with the decrease in the number of overlapping pentads during the  $FD_{SESR}$  and  $FD_{RZSM}$  episodes in the humid regions (Figure S8 in Supporting Information S1). Overall, these results indicate that the uncertainty in FD detection based on these two indicators is sensitive to the background aridity of the region, with a greater uncertainty noted for the humid regions. These associations can

be linked to higher initial RZSM conditions and extended memory of soil-moisture in wet (or humid) conditions (Liang & Yuan, 2021).

#### 4.3.2. Key Drivers of $FD_{SES}$ and $FD_{RZSM}$ Intensification in Different Climate Regimes

We used a machine learning-based random forest (RF) algorithm (Deo et al., 2017; Konapala & Mishra, 2020; Park et al., 2016; Rhee & Im, 2017; Sutanto et al., 2019) to determine the key drivers of  $FD_{SES}$  ( $FD_{RZSM}$ ) intensity in different evaporation regimes (see Methods). The gridded FD intensities within each evaporation regime are selected as predictand in the RF model development. The annual time series of mean FD intensity is derived for all the individual grids and then pooled together from all the grids within a given evaporation regime to be used as the RF model's predictand. The mean FD intensity for both the indicators (SES, and RZSM) are derived using the GLEAM dataset and fixed as a control with respect to which the influence of the climate variables are investigated. We include multiple temporal lags to capture the dynamics in the associations between the climate variables and FD intensification. For example, standardized anomalies of the climate variables, Pr, Tmax, VPD, and pi are derived at zero, 1, and 2 pentad lags (hereafter referred to as L0, L1, and L2) specific to each FD event onsets and their annual averages are used as predictors in the RF model. It should be noted that for any grid point, years with no FD events are excluded from the analysis. The key-drivers of  $FD_{RZSM}$  and  $FD_{SES}$  are determined based on the importance-score of these predictor variables. The importance-score of these climate variables is determined based on the percentage increase in mean squared error (%IncMSE) of prediction of the RF model corresponding to each predictor variable (see Methods). A higher magnitude of %IncMSE indicates relatively higher importance of the predictor variable. To determine the data-related uncertainties, the %IncMSE for all predictor variables is calculated using both ERA5 and MERRA2 datasets corresponding to the  $FD_{SES}$  and  $FD_{RZSM}$  events, as illustrated in Figure 4.

Substantial disparities arising from using two different datasets and indicators (ESR and RZSM) for a given evaporation regime can be noted among the selected key drivers. In the humid regimes, Pr(L1) is the key driver influencing the variation of  $FD_{SES}$  intensity, whereas Tmax(L0) is the key driver influencing  $FD_{RZSM}$  intensity based on both ERA5 and MERRA2 datasets. In the sub-humid regimes, while pi(L1) exhibits the most dominant control on  $FD_{SES}$  intensity based on both the datasets, Pr(L0) and Tmax (L0) are found to show the most substantial influence on  $FD_{RZSM}$  intensity based on the ERA5, and MERRA2 datasets, respectively. Similarly, Pr(L1) exhibits the most dominant control on  $FD_{SES}$  intensity in the semi-arid regimes, while Tmax(L1) shows the strongest influence on  $FD_{RZSM}$  intensity based on the ERA5 data set. On the other hand, pi(L1) and Tmax(L1) show the most dominant effect on  $FD_{SES}$  and  $FD_{RZSM}$  intensity in the MERRA2 data set. In the arid regimes, while Tmax(L1) exhibits the most dominant control on  $FD_{RZSM}$  intensity based on both the datasets, Pr(L2) and VPD(L2) is found to show the strongest influence on  $FD_{SES}$  intensity based on the ERA5, and MERRA2 datasets, respectively.

Overall, these results suggest a potential effect of background aridity on the uncertainties associated with the use of two distinct indicators of FD and the choice of different data sources. These disparities can also be linked to the dependence of transferability of soil temperature memory into atmospheric persistence on background aridity (Gerken et al., 2019), which significantly affects drying rates and, thereby, the depletion of ESR and RZSM differently.

## 5. Discussion and Conclusion

Our analyses provide global evidence that the employment of different flash drought definitions (or indicators) and datasets can lead to substantially disparate results associated with the FD characteristics and the key drivers. Climate variables, such as precipitation, temperature, vapor pressure deficit, and soil-moisture temperature coupling, exhibit a distinct control over flash drought evolution based on different FD indicators. The association between the flash drought indicators is sensitive to background aridity changes. The key drivers influencing the flash drought intensification in various climate regimes are found to be substantially different for different datasets and flash drought definitions.

The uncertainties associated with the choice of methodology and input data is noted in the FD frequency of occurrence and intensity. Using two distinct FD indicators, evaporative stress, and root-zone-soil moisture estimates, we found significant uncertainties associated with FD occurrences and rate of intensification in the humid southeastern parts of the US, northern parts of Europe, and Asia, some parts of central Asia, southernmost

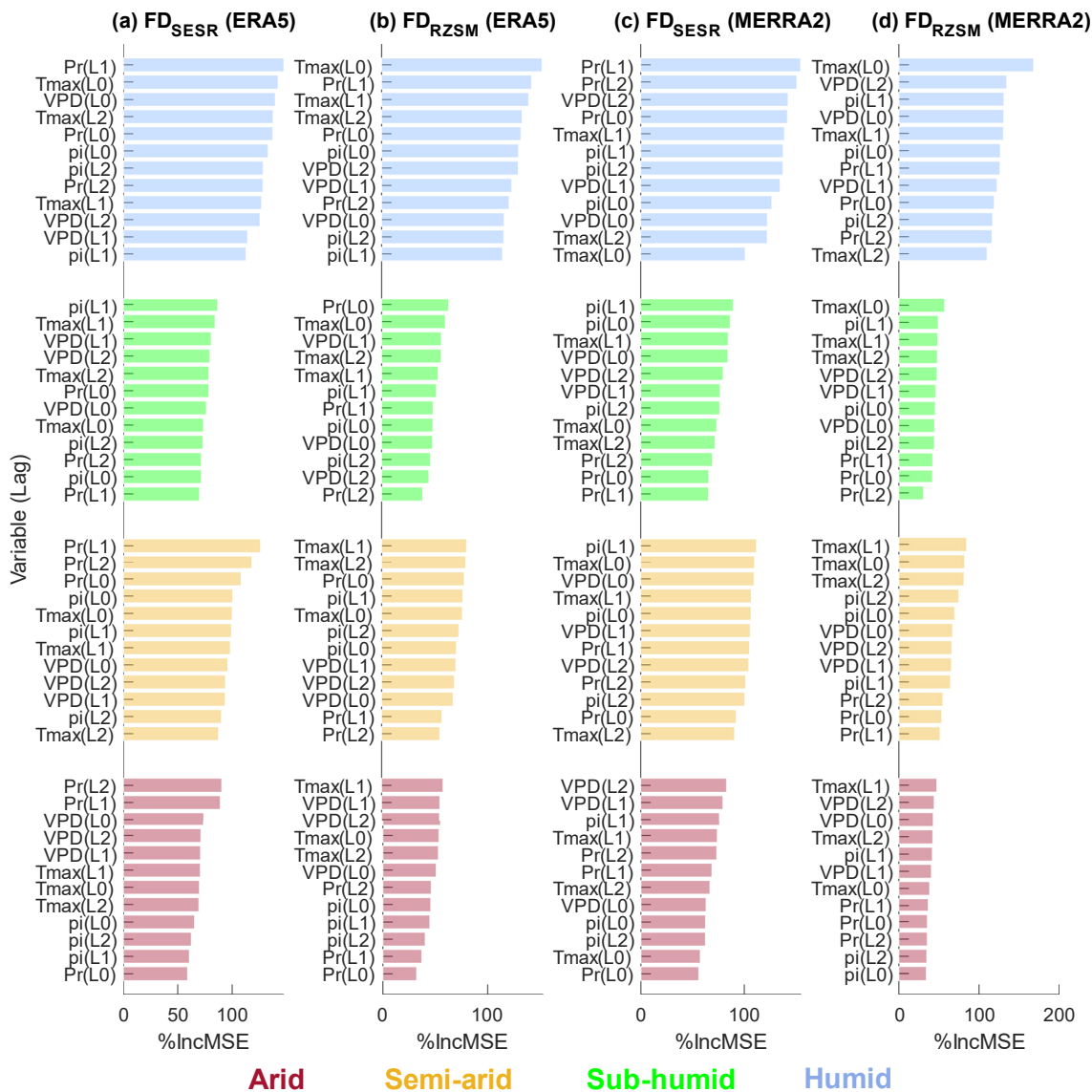


**Figure 4.** (a–d) bar-plots showing the key drivers influencing the variation of  $FD_{SESR}$  and  $FD_{RZSM}$  intensity for the different evaporation regimes. Note that both  $FD_{SESR}$  and  $FD_{RZSM}$  intensity are calculated based on the GLEAM dataset, whereas, the climate anomalies are calculated based on the (a and b) ERA5 and (c and d) MERRA2 datasets.

Africa, and Australia in the GLEAM data set, and in majority of the globe in both MERRA2 and ERA5 data set. We found that the control of climate variables on the FD evolution based on these two indicators are also very distinct. While the effect of climate variables on rapid intensification of evaporative stress occurs simultaneously, a cascading (time-delayed) climatic impact on the RZSM depletion is observed during the evolution of FDs. We also found that the uncertainties linked to different indicators are sensitive to the changes in background aridity and vary across different climate regimes. The relationship between evaporative stress and root-zone-soil moisture fails to explain most of the variance in each of these indicators specific to the flash drought episodes in the humid climate regimes. Besides that, the uncertainties associated with the key drivers influencing the FD intensification based on the two distinct indicators and different datasets in different climate regimes are found to be significant.

Our results suggest that global flash drought characteristics, drivers, and their temporal interactions vary across the evaporation regimes. These results reinforce the idea of existing trade-off between water availability and energy supply as a limiting factor for regulating evaporation, and site-specific connections of soil-specific water

retention capacities that control drying rates across different ecosystems (H. Wang et al., 2015). Therefore, caution should be exercised while addressing the robustness of the FD characteristics based on a single indicator and data set, especially in transitional and humid regimes where drying rates can be primarily driven by initial RZSM conditions and more extended memory of soil moisture in deeper (especially up to 1 m) layers (Entekhabi et al., 1996; Hagemann & Stacke, 2015; Hoffmann et al., 2020; Liang & Yuan, 2021; Seneviratne et al., 2006; H. Wang et al., 2015).

Overall, the results from this study will strengthen our perspective on flash droughts by improving our understanding of the underlying uncertainties and disparities associated with the use of a FD indicator and choice of data set in the context of their physical processes and essential predictors across different ecosystems. These results can also be implemented to refine our understanding of how FD hotspots vary across the definition and datasets in a multivariate setting (Mukherjee & Mishra, 2022). A key limitation of this study is the conversion of the datasets into a common spatial resolution. Although the purpose is to ensure comparability among the datasets, some influence of these underlying differences could still impact the results, in particular, for locations with varying topography, vegetation types, bodies of water, and along coast lines. In addition, due to limited scope, this study only compares two of the many indicators so far used in past studies to define flash drought (Lisonbee et al., 2021), which is why more research is needed to compare various other indices for exploring the related similarities and discrepancies among them. The findings can be further extended to explore a more robust indicator of flash drought that efficiently couples the rapid soil-moisture depletion rates in deeper layers with changes in atmospheric evaporative demand, and develop suitable forecasting tools focused on their direct implication on vegetation health (Pendergrass et al., 2020). By comparing two different flash drought definitions and using multiple datasets, the results from the study are expected to provide a broad and robust understanding of flash drought mechanisms and drivers globally. This is particularly important to highlight the advantages and limitations of the available flash drought definitions used by researchers and stakeholders (Christian, Basara, Otkin, & Hunt, 2019; Christian, Basara, Otkin, Hunt, et al., 2019; Christian et al., 2021; Mo & Lettenmaier, 2015, 2016; Otkin et al., 2018; L. Wang & Yuan, 2018). The new information gained in this study can be further extended to investigate the causal linkages of soil moisture memory length, vegetation fluxes, heatwaves and wildfires (Christian et al., 2020), and water use efficiency with FD characteristics across different ecosystems.

### Data Availability Statement

We are thankful for the data provided by the Global Land and Evaporation Amsterdam Model (GLEAM v3.3a; <https://www.gleam.eu/#datasets>), European Centre for Medium-Range Weather Forecasts Reanalysis 5 (<https://cds.climate.copernicus.eu/cdsapp#!/dataset/reanalysis-era5-single-levels?tab=form>), and Modern-Era Retrospective Analysis for Research and Applications, Version 2 available at [https://disc.gsfc.nasa.gov/datasets/M2SDNXSLV\\_5.12.4/summary](https://disc.gsfc.nasa.gov/datasets/M2SDNXSLV_5.12.4/summary) Precipitation and temperature and [https://disc.gsfc.nasa.gov/datasets/M2T1NXLND\\_5.12.4/summary](https://disc.gsfc.nasa.gov/datasets/M2T1NXLND_5.12.4/summary) for root-zone soil moisture and evaporative fluxes.

### References

- Anderson, M. C., Norman, J. M., Mecikalski, J. R., Otkin, J. A., & Kustas, W. P. (2007a). A climatological study of evapotranspiration and moisture stress across the continental United States based on thermal remote sensing: 1. Model formulation. *Journal of Geophysical Research*, 112(D10). <https://doi.org/10.1029/2006JD007506>
- Anderson, M. C., Norman, J. M., Mecikalski, J. R., Otkin, J. A., & Kustas, W. P. (2007b). A climatological study of evapotranspiration and moisture stress across the continental United States based on thermal remote sensing: 2. Surface moisture climatology. *Journal of Geophysical Research*, 112(D11), D11112. <https://doi.org/10.1029/2006JD007507>
- Anderson, M. C., Zolin, C. A., Sentelhas, P. C., Hain, C. R., Semmens, K., Tugrul Yilmaz, M., et al. (2016). The Evaporative Stress Index as an indicator of agricultural drought in Brazil: An assessment based on crop yield impacts. *Remote Sensing of Environment*, 174, 82–99. <https://doi.org/10.1016/j.rse.2015.11.034>
- Apurv, T., & Cai, X. (2020). Drought propagation in contiguous US watersheds: A process-based understanding of the role of climate and watershed properties. *Water Resources Research*, 56(9), e2020WR027755. <https://doi.org/10.1029/2020WR027755>
- Beltrami, H., & Kellman, L. (2003). An examination of short- and long-term air–ground temperature coupling. *Global and Planetary Change*, 38(3), 291–303. [https://doi.org/10.1016/S0921-8181\(03\)00112-7](https://doi.org/10.1016/S0921-8181(03)00112-7)
- Breiman, L. (2001). Random forests. *Machine Learning*, 45(1), 5–32. <https://doi.org/10.1023/a:1010933404324>
- Chen, L. G., Gottschalck, J., Hartman, A., Miskus, D., Tinker, R., & Artusa, A. (2019). Flash drought characteristics based on U.S. Drought monitor. *Atmosphere*, 10(9), 498. <https://doi.org/10.3390/atmos10090498>
- Christian, J. I., Basara, J. B., Hunt, E. D., Otkin, J. A., Furtado, J. C., Mishra, V., et al. (2021). Global distribution, trends, and drivers of flash drought occurrence. *Nature Communications*, 12(1), 6330. <https://doi.org/10.1038/s41467-021-26692-z>

### Acknowledgments

This study was supported by the National Science Foundation (NSF) awards # 1653841 and 1841629.



- Christian, J. I., Basara, J. B., Hunt, E. D., Otkin, J. A., & Xiao, X. (2020). Flash drought development and cascading impacts associated with the 2010 Russian heatwave. *Environmental Research Letters*, *15*(9), 094078. <https://doi.org/10.1088/1748-9326/ab9faf>
- Christian, J. I., Basara, J. B., Otkin, J. A., & Hunt, E. D. (2019). Regional characteristics of flash droughts across the United States. *Environmental Research Communications*, *1*(12), 125004. <https://doi.org/10.1088/2515-7620/ab50ca>
- Christian, J. I., Basara, J. B., Otkin, J. A., Hunt, E. D., Wakefield, R. A., Flanagan, P. X., & Xiao, X. (2019). A methodology for flash drought Identification: Application of flash drought frequency across the United States. *Journal of Hydrometeorology*, *20*(5), 833–846. <https://doi.org/10.1175/JHM-D-18-0198.1>
- Deo, R. C., Tiwari, M. K., Adamowski, J. F., & Quilty, J. M. (2017). Forecasting effective drought index using a wavelet extreme learning machine (W-ELM) model. *Stochastic Environmental Research and Risk Assessment*, *31*(5), 1211–1240. <https://doi.org/10.1007/s00477-016-1265-z>
- Entekhabi, D., Rodriguez-Iturbe, I., & Castelli, F. (1996). Mutual interaction of soil moisture state and atmospheric processes. *Journal of Hydrology*, *184*(1), 3–17. [https://doi.org/10.1016/0022-1694\(95\)02965-6](https://doi.org/10.1016/0022-1694(95)02965-6)
- Ford, T. W., & Labosier, C. F. (2017). Meteorological conditions associated with the onset of flash drought in the Eastern United States. *Agricultural and Forest Meteorology*, *247*, 414–423. <https://doi.org/10.1016/j.agrformet.2017.08.031>
- Ford, T. W., McRoberts, D. B., Quiring, S. M., & Hall, R. E. (2015). On the utility of in situ soil moisture observations for flash drought early warning in Oklahoma, USA. *Geophysical Research Letters*, *42*(22), 9790–9798. <https://doi.org/10.1002/2015GL066600>
- Forzieri, G., Miralles, D. G., Ciais, P., Alkama, R., Ryu, Y., Duveiller, G., et al. (2020). Increased control of vegetation on global terrestrial energy fluxes. *Nature Climate Change*, *10*(4), 356–362. <https://doi.org/10.1038/s41558-020-0717-0>
- Gerken, T., Ruddell, B. L., Yu, R., Stoy, P. C., & Drewry, D. T. (2019). Robust observations of land-to-atmosphere feedbacks using the information flows of FLUXNET. *Npj Climate and Atmospheric Science*, *2*(1), 1–10. <https://doi.org/10.1038/s41612-019-0094-4>
- Hagemann, S., & Stacke, T. (2015). Impact of the soil hydrology scheme on simulated soil moisture memory. *Climate Dynamics*, *44*(7), 1731–1750. <https://doi.org/10.1007/s00382-014-2221-6>
- Hanel, M., Rakovec, O., Markonis, Y., Máca, P., Samaniego, L., Kyselý, J., & Kumar, R. (2018). Revisiting the recent European droughts from a long-term perspective. *Scientific Reports*, *8*(1), 9499. <https://doi.org/10.1038/s41598-018-27464-4>
- Hao, Z., Singh, V. P., & Xia, Y. (2018). Seasonal drought prediction: Advances, challenges, and future prospects. *Reviews of Geophysics*, *56*, 108–141. <https://doi.org/10.1002/2016RG000549>
- He, M., Kimball, J. S., Yi, Y., Running, S., Guan, K., Jencso, K., et al. (2019). Impacts of the 2017 flash drought in the US Northern plains informed by satellite-based evapotranspiration and solar-induced fluorescence. *Environmental Research Letters*, *14*(7), 074019. <https://doi.org/10.1088/1748-9326/ab22c3>
- Hersbach, H., Bell, B., Berrisford, P., Hirahara, S., Horányi, A., Muñoz-Sabater, J., et al. (2020). The ERA5 global reanalysis. *Quarterly Journal of the Royal Meteorological Society*, *146*(730), 1999–2049. <https://doi.org/10.1002/qj.3803>
- Hoffmann, D., Gallant, A. J. E., & Arblaster, J. M. (2020). Uncertainties in drought from index and data selection. *Journal of Geophysical Research: Atmospheres*, *125*(18), e2019JD031946. <https://doi.org/10.1029/2019JD031946>
- Ionita, M., Tallaksen, L., Kingston, D., Stagge, J., Laaha, G., Van Lanen, H., et al. (2017). The European 2015 drought from a climatological perspective. *Hydrology and Earth System Sciences*, *21*(3), 1397–1419. <https://doi.org/10.5194/hess-21-1397-2017>
- Jin, C., Luo, X., Xiao, X., Dong, J., Li, X., Yang, J., & Zhao, D. (2019). The 2012 flash drought threatened US midwest agroecosystems. *Chinese Geographical Science*, *29*(5), 768–783. <https://doi.org/10.1007/s11769-019-1066-7>
- Konapala, G., & Mishra, A. (2020). Quantifying climate and catchment control on hydrological drought in the continental United States. *Water Resources Research*, *56*(1), e2018WR024620. <https://doi.org/10.1029/2018WR024620>
- Konapala, G., Mishra, A. K., Wada, Y., & Mann, M. E. (2020). Climate change will affect global water availability through compounding changes in seasonal precipitation and evaporation. *Nature Communications*, *11*(1), 3044. <https://doi.org/10.1038/s41467-020-16757-w>
- Koster, R. D., Schubert, S. D., Wang, H., Mahanama, S. P., & DeAngelis, A. M. (2019). Flash drought as captured by reanalysis data: Disentangling the contributions of precipitation deficit and excess evapotranspiration. *Journal of Hydrometeorology*, *20*(6), 1241–1258. <https://doi.org/10.1175/JHM-D-18-0242.1>
- Liang, M., & Yuan, X. (2021). Critical role of soil moisture memory in predicting the 2012 central United States flash drought. *Frontiers of Earth Science*, *9*. <https://doi.org/10.3389/feart.2021.615969>
- Lisonbee, J., Woloszyn, M., & Skumanich, M. (2021). Making sense of flash drought: Definitions, indicators, and where we go from here. *Journal of Applied and Service Climatology*, *2021*, 1–19. <https://doi.org/10.46275/joasc.2021.02.001>
- Mahto, S. S., & Mishra, V. (2020). Dominance of summer monsoon flash droughts in India. *Environmental Research Letters*, *15*(10), 104061. <https://doi.org/10.1088/1748-9326/abaf1d>
- Mallya, G., Zhao, L., Song, X. C., Niyogi, D., & Govindaraju, R. S. (2013). 2012 Midwest drought in the United States. *Journal of Hydrologic Engineering*, *18*(7), 737–745. [https://doi.org/10.1061/\(ASCE\)HE.1943-5584.0000786](https://doi.org/10.1061/(ASCE)HE.1943-5584.0000786)
- Martens, B., Schumacher, D. L., Wouters, H., Muñoz-Sabater, J., Verhoest, N. E., & Miralles, D. G. (2020). Evaluating the surface energy partitioning in ERA5. *Geoscientific Model Development Discussions*, 1–35.
- McColl, K. A., Alemohammad, S. H., Akbar, R., Konings, A. G., Yueh, S., & Entekhabi, D. (2017). The global distribution and dynamics of surface soil moisture. *Nature Geoscience*, *10*(2), 100–104. <https://doi.org/10.1038/ngeo2868>
- Miralles, D. G., Berg, M. J., van den Teuling, A. J., & de Jeu, R. A. M. (2012). Soil moisture-temperature coupling: A multiscale observational analysis. *Geophysical Research Letters*, *39*(21). <https://doi.org/10.1029/2012GL053703>
- Miralles, D. G., Holmes, T. R. H., De Jeu, R. A. M., Gash, J. H., Meesters, A. G. C. A., & Dolman, A. J. (2011). Global land-surface evaporation estimated from satellite-based observations. *Hydrology and Earth System Sciences*, *15*(2), 453–469. <https://doi.org/10.5194/hess-15-453-2011>
- Mishra, A. K., & Singh, V. P. (2010). A review of drought concepts. *Journal of Hydrology*, *391*(1), 202–216. <https://doi.org/10.1016/j.jhydrol.2010.07.012>
- Mishra, V., Aadhar, S., & Mahto, S. S. (2021). Anthropogenic warming and intraseasonal summer monsoon variability amplify the risk of future flash droughts in India. *Npj Climate and Atmospheric Science*, *4*(1), 1–10. <https://doi.org/10.1038/s41612-020-00158-3>
- Mo, K. C., & Lettenmaier, D. P. (2015). Heat wave flash droughts in decline. *Geophysical Research Letters*, *42*(8), 2823–2829. <https://doi.org/10.1002/2015GL064018>
- Mo, K. C., & Lettenmaier, D. P. (2016). Precipitation deficit flash droughts over the United States. *Journal of Hydrometeorology*, *17*(4), 1169–1184. <https://doi.org/10.1175/JHM-D-15-0158.1>
- Mukherjee, S., Mishra, A., & Trenberth, K. E. (2018). Climate change and drought: A perspective on drought indices. *Current Climate Change Reports*, *4*(2), 145–163. <https://doi.org/10.1007/s40641-018-0098-x>
- Mukherjee, S., & Mishra, A. K. (2021). Increase in compound drought and heatwaves in a warming world. *Geophysical Research Letters*, *48*(1), e2020GL090617. <https://doi.org/10.1029/2020GL090617>

- Mukherjee, S., & Mishra, A. K. (2022). A multivariate flash drought indicator for identifying global hotspots and associated climate controls. *Geophysical Research Letters*, 49(2), e2021GL096804. <https://doi.org/10.1029/2021GL096804>
- Noguera, I., Domínguez-Castro, F., & Vicente-Serrano, S. M. (2021). Flash drought response to precipitation and atmospheric evaporative demand in Spain. *Atmosphere*, 12(2), 165. <https://doi.org/10.3390/atmos12020165>
- Osman, M., Zaitchik, B. F., Badr, H. S., Christian, J. I., Tadesse, T., Otkin, J. A., & Anderson, M. C. (2020). Flash drought onset over the Contiguous United States: Sensitivity of inventories and trends to quantitative definitions. *Hydrology and Earth System Sciences Discussions*, 1–21. <https://doi.org/10.5194/hess-2020-385>
- Otkin, J. A., Anderson, M. C., Hain, C., Svoboda, M., Johnson, D., Mueller, R., et al. (2016). Assessing the evolution of soil moisture and vegetation conditions during the 2012 United States flash drought. *Agricultural and Forest Meteorology*, 218–219, 230–242. <https://doi.org/10.1016/j.agrformet.2015.12.065>
- Otkin, J. A., Svoboda, M., Hunt, E. D., Ford, T. W., Anderson, M. C., Hain, C., & Basara, J. B. (2018). Flash droughts: A review and assessment of the challenges imposed by rapid-onset droughts in the United States. *Bulletin of the American Meteorological Society*, 99(5), 911–919. <https://doi.org/10.1175/BAMS-D-17-0149.1>
- Park, S., Im, J., Jang, E., & Rhee, J. (2016). Drought assessment and monitoring through blending of multi-sensor indices using machine learning approaches for different climate regions. *Agricultural and Forest Meteorology*, 216, 157–169. <https://doi.org/10.1016/j.agrformet.2015.10.011>
- Parker, T., Gallant, A., Hobbins, M., & Hoffmann, D. (2021). Flash drought in Australia and its relationship to evaporative demand. *Environmental Research Letters*, 16(6), 064033. <https://doi.org/10.1088/1748-9326/abfe2c>
- Pendergrass, A. G., Meehl, G. A., Pulwarty, R., Hobbins, M., Hoell, A., AghaKouchak, A., et al. (2020). Flash droughts present a new challenge for subseasonal-to-seasonal prediction. *Nature Climate Change*, 10(3), 191–199. <https://doi.org/10.1038/s41558-020-0709-0>
- Raymond, C., Horton, R. M., Zscheischler, J., Martius, O., AghaKouchak, A., Balch, J., et al. (2020). Understanding and managing connected extreme events. *Nature Climate Change*, 10(7), 611–621. <https://doi.org/10.1038/s41558-020-0790-4>
- Reichle, R. H., Draper, C. S., Liu, Q., Girotto, M., Mahanama, S. P. P., Koster, R. D., & Lannoy, G. J. M. D. (2017). Assessment of MERRA-2 land surface hydrology estimates. *Journal of Climate*, 30(8), 2937–2960. <https://doi.org/10.1175/JCLI-D-16-0720.1>
- Rhee, J., & Im, J. (2017). Meteorological drought forecasting for ungauged areas based on machine learning: Using long-range climate forecast and remote sensing data. *Agricultural and Forest Meteorology*, 237, 105–122. <https://doi.org/10.1016/j.agrformet.2017.02.011>
- Seneviratne, S. I., Corti, T., Davin, E. L., Hirschi, M., Jaeger, E. B., Lehner, I., et al. (2010). Investigating soil moisture–climate interactions in a changing climate: A review. *Earth-Science Reviews*, 99(3), 125–161. <https://doi.org/10.1016/j.earscirev.2010.02.004>
- Seneviratne, S. I., Koster, R. D., Guo, Z., Dirmeyer, P. A., Kowalczyk, E., Lawrence, D., et al. (2006). Soil moisture memory in AGCM Simulations: Analysis of global land–atmosphere coupling experiment (GLACE) data. *Journal of Hydrometeorology*, 7(5), 1090–1112. <https://doi.org/10.1175/JHM533.1>
- Su, J., Gou, X., HilleRisLambers, J., Deng, Y., Fan, H., Zheng, W., et al. (2021). Increasing climate sensitivity of subtropical conifers along an aridity gradient. *Forest Ecology and Management*, 482, 118841. <https://doi.org/10.1016/j.foreco.2020.118841>
- Sutanto, S. J., van der Weert, M., Wanders, N., Blauhut, V., & Van Lanen, H. A. J. (2019). Moving from drought hazard to impact forecasts. *Nature Communications*, 10(1), 4945. <https://doi.org/10.1038/s41467-019-12840-z>
- Svoboda, M., LeComte, D., Hayes, M., Heim, R., Gleason, K., Angel, J., et al. (2002). The drought MONITOR. *Bulletin of the American Meteorological Society*, 83(8), 1181–1190. <https://doi.org/10.1175/1520-0477-83.8.1181>
- Vicente-Serrano, S. M., McVicar, T. R., Miralles, D. G., Yang, Y., & Tomas-Burguera, M. (2020). Unraveling the influence of atmospheric evaporative demand on drought and its response to climate change. *WIREs Climate Change*, 11(2), e632. <https://doi.org/10.1002/wcc.632>
- Wang, H., Rogers, J. C., & Munroe, D. K. (2015). Commonly used drought indices as indicators of soil moisture in China. *Journal of Hydrometeorology*, 16(3), 1397–1408. <https://doi.org/10.1175/jhm-d-14-0076.1>
- Wang, L., & Yuan, X. (2018). Two types of flash drought and their connections with seasonal drought. *Advances in Atmospheric Sciences*, 35(12), 1478–1490. <https://doi.org/10.1007/s00376-018-8047-0>
- Wang, L., Yuan, X., Xie, Z., Wu, P., & Li, Y. (2016). Increasing flash droughts over China during the recent global warming hiatus. *Scientific Reports*, 6(1), 30571. <https://doi.org/10.1038/srep30571>
- Yuan, X., Wang, L., Wu, P., Ji, P., Sheffield, J., & Zhang, M. (2019). Anthropogenic shift towards higher risk of flash drought over China. *Nature Communications*, 10(1), 4661. <https://doi.org/10.1038/s41467-019-12692-7>
- Zscheischler, J., Martius, O., Westra, S., Bevacqua, E., Raymond, C., Horton, R. M., et al. (2020). A typology of compound weather and climate events. *Nature Reviews Earth & Environment*, 1(7), 333–347. <https://doi.org/10.1038/s43017-020-0060-z>

## References From the Supporting Information

- Gevaert, A. I., Miralles, D. G., de Jeu, R. A. M., Schellekens, J., & Dolman, A. J. (2018). Soil moisture-temperature coupling in a set of land surface models. *Journal of Geophysical Research: Atmospheres*, 123(3), 1481–1498. <https://doi.org/10.1002/2017JD027346>
- Jia, A., Liang, S., Jiang, B., Zhang, X., & Wang, G. (2018). Comprehensive assessment of global surface Net radiation Products and uncertainty analysis. *Journal of Geophysical Research: Atmospheres*, 123(4), 1970–1989. <https://doi.org/10.1002/2017JD027903>
- Liu, X., He, B., Guo, L., Huang, L., & Chen, D. (2020). Similarities and differences in the mechanisms causing the European summer heatwaves in 2003, 2010, and 2018. *Earth's Future*, 8(4), e2019EF001386. <https://doi.org/10.1029/2019EF001386>
- Lu, J., Sun, G., McNulty, S. G., & Amatya, D. M. (2005). A comparison of six potential evapotranspiration methods for regional Use in the southeast-ern United States I. *JAWRA Journal of the American Water Resources Association*, 41(3), 621–633. <https://doi.org/10.1111/j.1752-1688.2005.tb03759.x>
- Miralles, D. G., van den Berg, M. J., Teuling, A. J., & de Jeu, R. A. M. (2012). Soil moisture-temperature coupling: A multiscale observational analysis. *Geophysical Research Letters*, 39(21). <https://doi.org/10.1029/2012GL053703>
- Shukla, P., Skeg, J., Buendia, E. C., Masson-Delmotte, V., Pörtner, H.-O., Roberts, D., et al. (2019). *Climate change and land: An IPCC special report on climate change, desertification, land degradation, sustainable land management, food security, and greenhouse gas fluxes in terrestrial ecosystems*.
- Unep, N. M., & Thomas, D. (1992). *World atlas of desertification* (pp. 15–45). Edward Arnold.
- Wang, D., & Tang, Y. (2014). A one-parameter Budyko model for water balance captures emergent behavior in Darwinian hydrologic models. *Geophysical Research Letters*, 41(13), 4569–4577. <https://doi.org/10.1002/2014GL060509>
- Yuan, W., Zheng, Y., Piao, S., Ciais, P., Lombardozzi, D., Wang, Y., et al. (2019). Increased atmospheric vapor pressure deficit reduces global vegetation growth. *Science Advances*, 5(8), eaax1396. <https://doi.org/10.1126/sciadv.aax1396>